ACS APPLIED MATERIALS & INTERFACES

Research Article

www.acsami.org

# Revealing the Crystalline Integrity of Wafer-Scale Graphene on $SiO_2$/Si: An Azimuthal RHEED Approach

Zonghuan Lu, Xin Sun,* Yu Xiang, Morris A. Washington, Gwo-Ching Wang, and Toh-Ming Lu

Department of Physics, Applied Physics, and Astronomy, and Center for Materials, Devices, and Integrated Systems, Rensselaer Polytechnic Institute, Troy, New York 12180, United States

Supporting Information

**ABSTRACT:** The symmetry of graphene is usually determined by a low-energy electron diffraction (LEED) method when the graphene is on the conductive substrates, but LEED cannot handle graphene transferred to $SiO_2$/Si substrates due to the charging effect. While transmission electron microscopy can generate electron diffraction on post-transferred graphene, this method is too localized. Herein, we employed an azimuthal reflection high-energy electron diffraction (RHEED) method to construct the reciprocal space mapping and determine the symmetry of wafer-size graphene both pre- and post-transfer. In this work, single-crystalline Cu(111) films were prepared on sapphire(0001) and spinel(111) substrates with sputtering. Then the graphene was epitaxially grown on single-crystalline Cu(111) films with a low pressure chemical vapor deposition. The reciprocal space mapping using azimuthal RHEED confirmed that the graphene grown on Cu(111) films was single-crystalline, no matter the form of the monolayer or multilayer structure. While the Cu(111) film grown on sapphire(0001) may occasionally consist of 60° in-plane rotational twinning, the reciprocal space mapping revealed that the in-plane orientation of graphene grown atop was not affected. The proposed method for checking the crystalline integrity of the post-transferred graphene sheets is an important step in the realization of the graphene as a platform to fabricate electronic and optoelectronic devices.

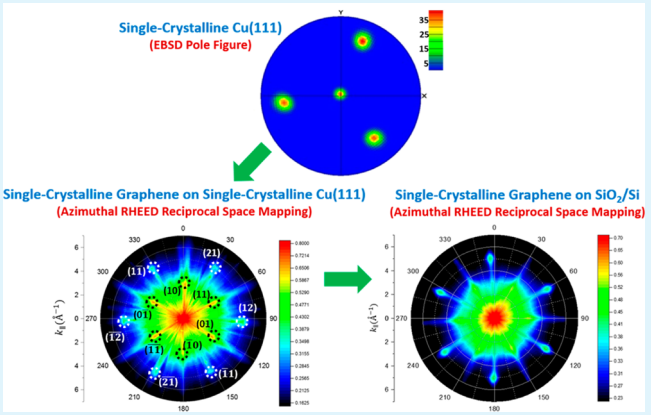


**KEYWORDS:** *epitaxial Cu, twinning, single-crystalline graphene, post-transfer, RHEED, symmetry, reciprocal space mapping*

## INTRODUCTION

Owing to its remarkable physical properties, such as high carrier mobility, high thermal and electrical conductivity, and high optical transparency, graphene has attracted worldwide attention since Geim and Novoselov's report in 2004.[1] Since then, a great deal of effort has been devoted to fabrication of high-quality graphene that has characteristics of single crystallinity, monolayer, and scalability.[2−9] Among these qualities, single crystallinity is of foremost importance. Bilayer and few-layer graphene, if grown in a controlled manner, might have special uses, such as bandgap engineering, as some researchers have purposely pursued them.[10−13] But polycrystalline graphene has often been considered undesirable for electronics because the grain boundaries would undermine the extraordinary properties people expect to obtain from single-crystal graphene. To date, chemical vapor deposition (CVD) is the most widely used method to produce high-quality graphene on a large scale by reducing a gaseous carbon-containing compound with the aid of a metal/nonmetal (Cu, Ni, Co, Ir, Ru, Ge, etc.) catalyst.[3,14−17] Given the fact that graphene directly forms on top of this catalyst substrate, it implies that one would be able to obtain wafer-scale single-crystalline graphene if a wafer-scale single-crystalline catalyst substrate is used. In this regard, the Cu(111) surface has been a favorable choice due to its advantages in symmetry matching with graphene, effectiveness for catalysis, low carbon solubility, and relative ease in preparing a single-crystalline form.[18−21] Several oxide wafers, including sapphire ($Al_2O_3$), magnesium oxide (MgO), and spinel ($MgAl_2O_4$), have been used to grow single-crystalline Cu(111) films.[2,19,22,23] While single-crystalline Cu(111) indeed can be achieved in this way, some have frequently encountered a 60° in-plane rotational twinning in these Cu films. Some studies indicate that the graphene growth direction is rotated 30° across the Cu twin boundaries which also serve as the carbon segregation and nucleation sites.[20] As a result, several methods have been explored, such as rigorous surface pretreatment[24,25] and using single-crystalline Cu sputtering target,[10] to remove the twinning in Cu films since it appears to be a concern for the growth of single-crystalline graphene.

As stressed previously, the single crystallinity of graphene is a key to its successful use in electronics. Currently, the low-

Received: January 26, 2017
Accepted: June 16, 2017
Published: June 16, 2017





DOI: 10.1021/acsami.7b01370
ACS Appl. Mater. Interfaces XXXX, XXX, XXX−XXX

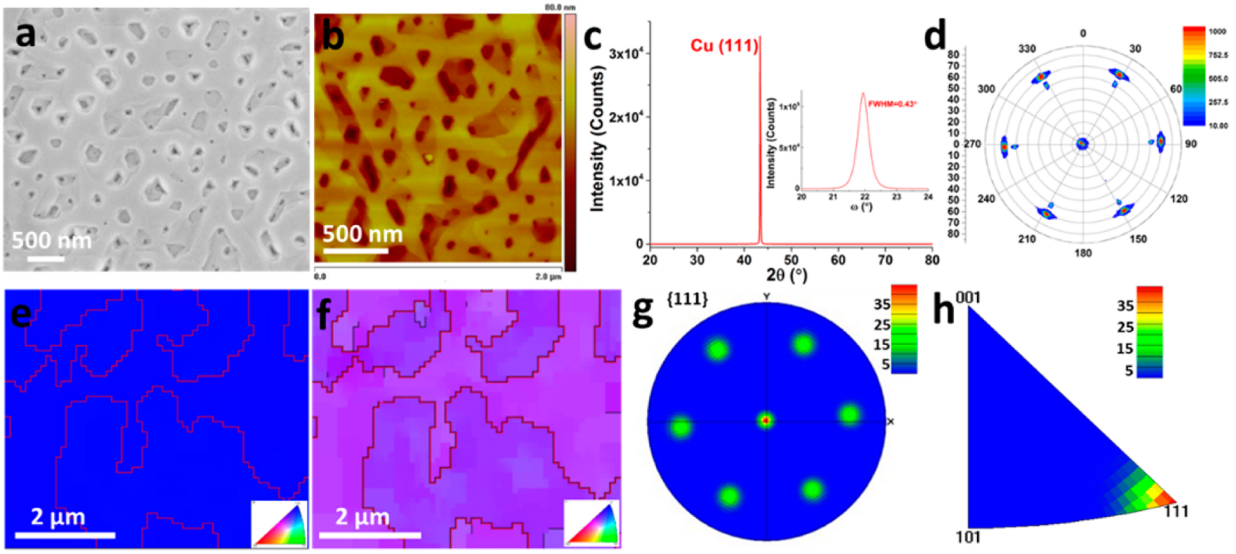


**Figure 1.** (a) SEM image and (b) AFM image of the ∼900 nm Cu film grown on a sapphire(0001) substrate. The root-mean-square surface roughness is ∼6−9 nm. (c) XRD $\theta$-$2\theta$ scan of the Cu film grown on a sapphire(0001) substrate; the inset shows the rocking curve for the Cu(111) diffraction. (d) XRD Cu{111} pole figure of the Cu film grown on a sapphire(0001) substrate. The outer six poles and inner six poles are from Cu and sapphire, respectively. (e, f) EBSD crystallographic orientation maps of the Cu film grown on a sapphire(0001) substrate using (e) IPF-Z mapping component and (f) IPF-Y mapping component, respectively. (g) EBSD Cu{111} pole figure of the Cu film grown on a sapphire(0001) substrate. (h) IPF-Z of the Cu film grown on a sapphire(0001) substrate.

energy electron diffraction (LEED) technique is the most-used technique to reveal the symmetry of graphene after its growth on conductive substrates, such as catalyst metals. However, this method, with a beam energy of 10−300 eV, becomes inapplicable after the graphene is transferred to nonconductive substrates, such as $SiO_2$, due to the severe charging problem.[26] One may argue that the crystallinity is already determined during graphene growth and would not be altered by the transfer. But there is no convincing evidence to confirm it. In fact, the quality degradation of graphene post-transferred has long been a concern. Efforts have been put toward either improving the transfer process or circumventing the transfer by direct growth of graphene on dielectric substrates.[27−32] The selected area electron diffraction (SAED) technique in transmission electron microscopy (TEM) can be used to characterize post-transferred graphene.[33] However, TEM is a local probe, and its low throughput does not allow it to characterize graphene over a large scale. Furthermore, the substrates for graphene growth are not limited to metals. Insulating substrates, such as sapphire, $Si_3N_4$, and $SiO_2$, have all been used as substrates for the direct growth of graphene.[29,31,32] Unfortunately for these as-grown graphene sheets, the LEED method is not an option because of the charging issue. Therefore, a characterization method capable of revealing the crystallinity of large-scale graphene sheets on selective insulating substrates would be an attractive solution to the above needs.

Previously, we reported an azimuthal reflection high-energy electron diffraction (RHEED) method that could tell the symmetry of graphene on both conductive and insulating substrates.[34] The principle for this azimuthal RHEED is similar to Satapathy's work.[35] In our previous report,[34] we described the concept, theory, and procedures of the method and tested the feasibility of this method with a commercial polycrystalline graphene sample. Herein, we further explore this subject by verifying our theory with single crystalline graphene samples prepared in our laboratory. In this work, we demonstrate the epitaxial growth of Cu(111) films on sapphire(0001) and spinel(111) substrates using DC sputtering and postdeposition annealing. While twinning cannot always be completely removed on sapphire(0001) substrates, we do obtain enlarged twin domains at the size of several hundreds of micrometers. On the other hand, single-crystalline Cu(111) films can be obtained on spinel(111) substrates on a consistent basis. This study, unlike previous reports regarding the role of Cu twinning on graphene growth, suggests that the 60° in-plane rotational twinning does not affect the crystallographic properties of graphene grown atop, although the twinning may promote the graphene to grow in a multilayer format. In this study, the crystallinity of both the pre- and post-transferred graphene samples is characterized with the azimuthal RHEED method. For the pretransferred graphene, our azimuthal RHEED method is similar to LEED, except for the beam incidence angle (glancing for RHEED and normal for LEED). For the post-transferred graphene to a $SiO_2$/Si substrate, however, the azimuthal RHEED is much more powerful than LEED. The high beam energy in keV or tens of keV range of RHEED is more tolerant to the electron charging effect. In brief, the charging effect in electron diffraction is a result mainly coming from the competition between the electrons injected into the insulator and the secondary electron emission, which depends on the incident energy.[36,37] In RHEED, the strong forward scattering and a relative reduction of inelastic scattering that gives rise to the secondary electron emission makes it more tolerant to surface charging that may affect the electron diffraction path.[38] Hence, RHEED is feasible to characterize graphene sheets on $SiO_2$/Si substrates with the $SiO_2$ layer as thick as several hundreds of nanometer. Furthermore, a 1 mm diameter electron beam in RHEED strikes the graphene surface from a glancing angle (∼1°), making this technique extremely valuable to investigate the crystalline integrity of wafer scale graphene samples. Considering that many graphene-based electronic devices are and will continue to be fabricated on silicon oxides,[13,39−44] we believe that this azimuthal RHEED


DOI: 10.1021/acsami.7b01370
ACS Appl. Mater. Interfaces XXXX, XXX, XXX−XXX

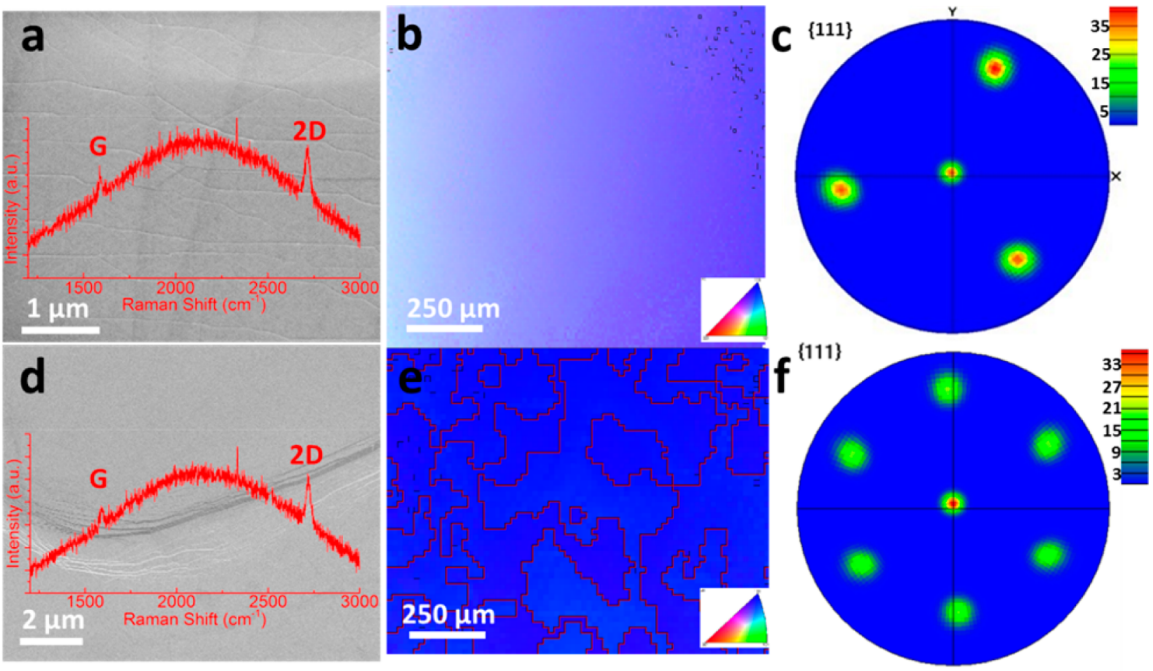


**Figure 2.** (a) SEM image of the Cu film without twin domains on a sapphire(0001) substrate after thermal annealing and graphene growth; overlay shows a Raman spectrum acquired from this sample. G and 2D peaks are labeled in the spectrum. (b) EBSD crystallographic orientation map of the Cu film without twin domains on a sapphire(0001) after thermal annealing and graphene growth using IPF-Z mapping component. (c) EBSD Cu{111} pole figure of the Cu film without twin domains on a sapphire(0001) after thermal annealing and graphene growth. (d) SEM image of the Cu film with twin domains on a sapphire(0001) substrate after thermal annealing and graphene growth; overlay shows a Raman spectrum acquired from this sample. (e) EBSD crystallographic orientation map of the Cu film with twin domains on a sapphire(0001) substrate after thermal annealing and graphene growth using IPF-Z mapping component. (f) EBSD Cu {111} pole figure of the Cu film with twin domains on a sapphire(0001) after thermal annealing and graphene growth.

technique could be a valuable tool to check the structure of graphene on oxides before making devices.

## RESULTS AND DISCUSSION

Figure 1a shows the scanning electron microscopy (SEM) image of an as-sputtered 900 nm thick Cu film on sapphire(0001). Widely spread submicron pits can be found on the otherwise flat Cu surface. Figure 1b shows the atomic force microscopy (AFM) image of the same Cu surface where a similar morphology is revealed. The measured root-mean-square (RMS) surface roughness for this Cu film is 6−9 nm. The X-ray diffraction (XRD) $\theta$-$2\theta$ scan, shown in Figure 1c, presents only one Cu (111) peak at $2\theta$ of 43.4°. The absence of any other diffraction peaks implies that the Cu film is highly textured with the out-of-plane orientation along <111>. The rocking curve of this Cu (111) peak, displayed as the inset of Figure 1c, shows a small full-width-at-half-maximum (fwhm) of ∼0.43°, suggesting the Cu film has a superior crystal quality. To find out the texture of this Cu film and its crystallographic relationship with the sapphire substrate, the Cu {111} X-ray pole figure was collected. Shown in Figure 1d, there are six symmetrical poles at the polar angle $\chi$ of ∼70° with an azimuthal angle $\varphi$ of 60° apart, which confirms that the Cu film is in single-crystalline form but with in-plane rotational twin domains.[24,45] Furthermore, the similarity in intensity strength of these six poles indicates that the twin domains may account for approximately half of the Cu film. In addition to the Cu {111} poles, there are six weaker and symmetrical poles at $\chi$ of ∼62° in the pole figure. These poles are attributed to the $\{2\bar{1}\bar{1}3\}$ crystal planes of sapphire. Based on the alignment of these two sets of poles, it can be concluded that the Cu film is epitaxially aligned with the sapphire substrate, that is, Cu(111) $[\bar{2}11]$ ‖ sapphire(0001) $[\bar{2}110]$. In order to estimate the size of the Cu twin domains and the microstructures of this epitaxial Cu(111) film, electron backscatter diffraction (EBSD) analysis was conducted. Figure 1e shows the crystallographic orientation map of the Cu film using the inverse pole figure (IPF)-Z component, which correlates the spatial crystallographic orientations with respect to the normal of sample surface. The uniform blueness in Figure 1e suggests the sample normal direction to be ⟨111⟩ across the whole map, consistent with the XRD result. Figure 1f shows an in-plane crystallographic orientation map using the IPF-Y mapping component. There are two regions represented by two different, yet close, colors, separated by grain boundaries represented by the red contours. The grain boundaries are the coincidence site of lattice boundaries with a sigma ($\Sigma$) value of 3, indicating a 60° in-plane rotation of the crystal orientation. The distribution of the grain boundary misorientation angles is shown in Figure S1. One can see that the majority of the grain boundaries are (111) twin boundaries with a mis-orientation angular of 58−60°. The remaining grain boundaries have a small mis-orientation angle less than 5°. Per the twin boundaries shown in Figure 1e,f, the size of these twin domains is estimated to be several micrometers. Figure 1g,h show the Cu{111} EBSD pole figure and IPF in the sample normal direction, respectively, further confirming the presence of 60° in-plane rotational twin domains and ⟨111⟩ out-of-plane orientation. The Cu film sputtered on spinel(111) is overall similar to that on sapphire(0001), except that the twin domains only account for a tiny portion of the Cu film. The epitaxial alignment between Cu film and the spinel substrate is Cu(111)[100] ‖


DOI: 10.1021/acsami.7b01370
ACS Appl. Mater. Interfaces XXXX, XXX, XXX−XXX

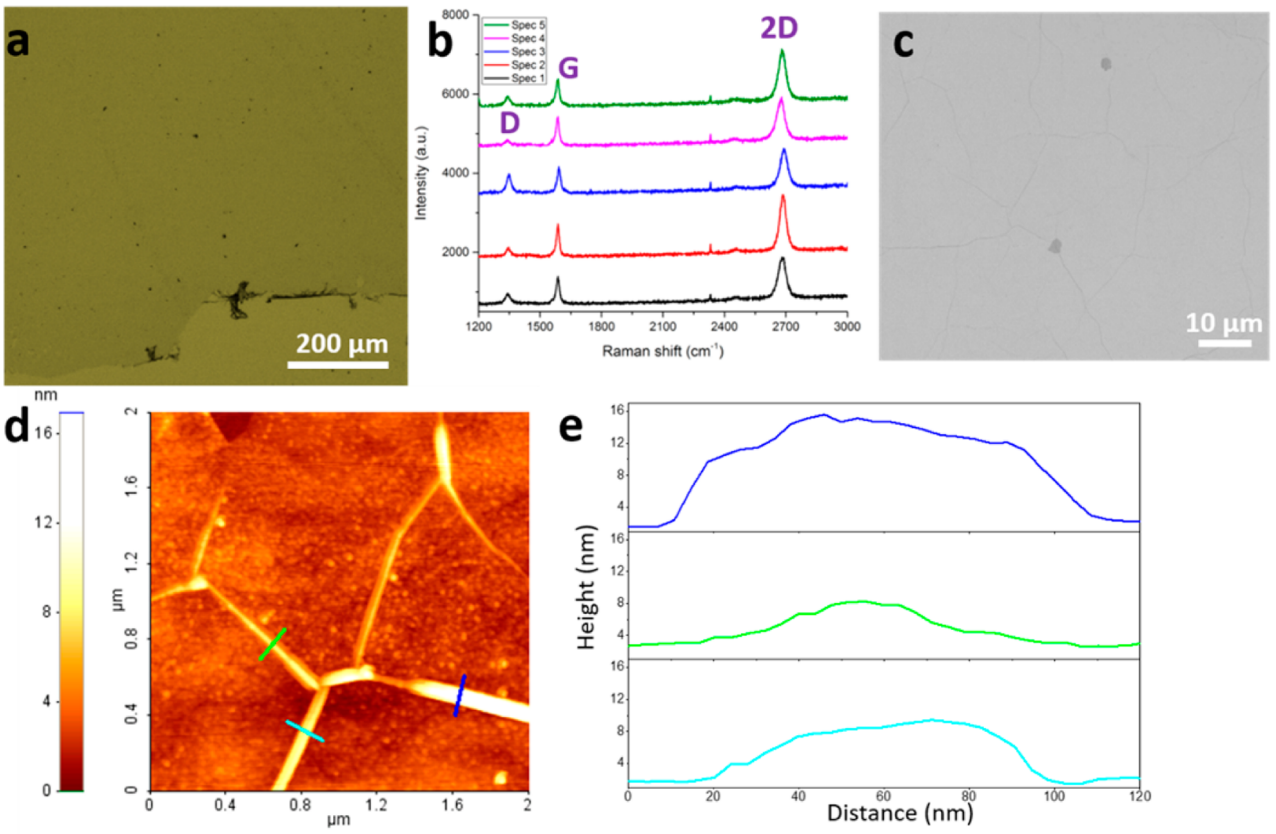


**Figure 3.** (a) Optical image of the continuous monolayer graphene sheet transferred to a $SiO_2$/Si substrate. (b) Collected Raman spectra from random areas on the continuous monolayer graphene sheet transferred to a $SiO_2$/Si substrate. (c) SEM image of the monolayer graphene sheet transferred to a $SiO_2$/Si substrate. (d) AFM image and (e) three line scan profiles across the wrinkles in the monolayer graphene transferred to a $SiO_2$/Si substrate.

spinel(111)[100]. Detailed results regarding Cu film sputtered on spinel(111) can be found in Figures S2−S4 in the Supporting Information.

The postdeposition annealing of Cu films and the graphene growth were conducted in the same furnace and the latter immediately followed the former. The thermal annealing is designed to better position the Cu films for graphene growth by recrystallizing and smoothening out the Cu films. In some cases, the twin domains can be completely removed after this process. For example, Figure 2a shows the SEM image of a Cu film, without twin domains, on sapphire(0001), after the thermal annealing and the graphene growth. Clearly different from its original form, the Cu surface is smooth and free of pits. The inset in Figure 2a shows a Raman spectrum collected from this surface with a 514 nm laser line. Characteristic 2D (2712 $cm^{-1}$) and G (1591 $cm^{-1}$) peaks of graphene can be identified, confirming the occurrence of graphene growth on this surface. Given the high intensity ratio of 2D/G, along with the fact that no noticeable defect D peak can be detected, it is inferred that the graphene is monolayer and is of high quality. The central bump-up of the spectral profile is believed to be caused by the surface plasmon emission of Cu.[46] Given that the energy gap between Fermi level and d state of Cu is around 2.1 eV or 590 nm,[47] theoretically there would be a broad emission peak centered at 2506 $cm^{-1}$ under an excitation of 514 nm. In this work, the emission is experimentally observed around 2200 $cm^{-1}$, implying that the actual Cu emission peak is at around 580 nm for this particular Cu film. We believe this deviation is very reasonable, considering that the fwhm of Cu emission peak in ref 47 is about 100 nm wide. Figure 2b shows the EBSD crystallographic orientation map of this Cu film using the IPF-Z component. The super homogeneity of color in this map indicates that the twin boundaries have been completely removed after the thermal annealing and the graphene growth. The Cu{111} EBSD pole figure in Figure 2c presents a clean 3-fold symmetry, also confirming that the film is free of twin domains.

On the other hand, it has been found that the twin domains sometimes are tough to remove for the Cu film on sapphire(0001). Figure 2d shows the SEM image of a Cu film, still with twin domains, on sapphire(0001) after the thermal annealing and the graphene growth. Despite the film is smooth and free of pits as in the case of Figure 2a, a boundary groove can be clearly seen in the middle of this image. Nonetheless, these grooves do not seem to affect the graphene growth, since high-quality and monolayer graphene can still be found on this surface as evident by the Raman spectrum inset of Figure 2d. The G and 2D peak are located at 1588 and 2719 $cm^{-1}$, respectively. The EBSD IPF-Z crystallographic orientation map in Figure 2e confirms that these boundaries are the same twin boundaries as prior to the thermal annealing and the graphene growth. However, note that the size of twin domains increases approximately by 2 orders of magnitude. The Cu{111} EBSD pole figure in Figure 2f confirms that these twin domains remain to be in-plane rotated by 60°, and the fraction of these twin domains is still about half of the Cu film, similar to that in the as-sputtered Cu film. Overall, it is found that the status of Cu films, twin-free or twinned, after the


DOI: 10.1021/acsami.7b01370
ACS Appl. Mater. Interfaces XXXX, XXX, XXX−XXX

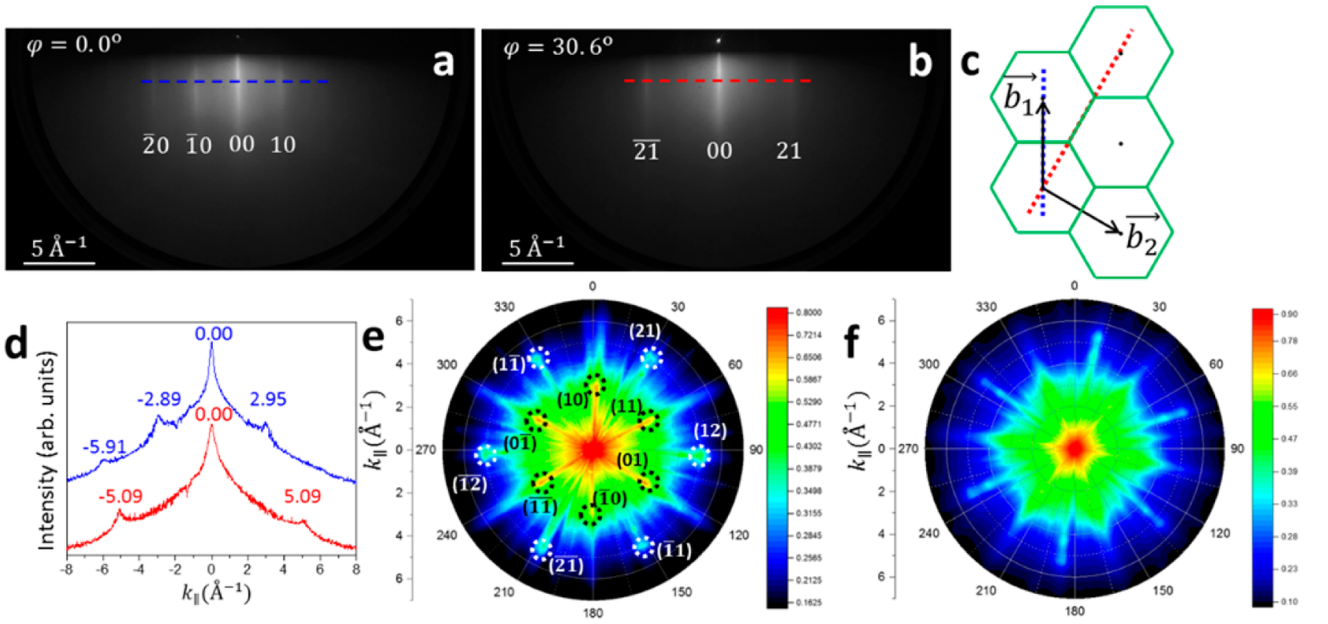


**Figure 4.** (a, b) RHEED patterns of the monolayer graphene on a twin-free Cu(111) film when the electron beam incident at azimuthal angles $\varphi$ = 0 and 30.6°, respectively. The two-dimensional Miller index ($hk$) is labeled in (a) and (b). The $\vec{b}_1$ and $\vec{b}_2$ are unit vectors in the reciprocal space. The scale bar is 5 Å$^{-1}$. (c) Schematics showing the directions of blue and red dashed lines in the reciprocal space (RHEED patterns) of a monolayer graphene shown in (a) and (b), respectively. (d) Intensity profiles along the blue and red dashed lines in (a) and (b), respectively. (e) Experimentally acquired reciprocal space structure of the monolayer graphene on a twin-free Cu(111) film. The ($hk$) pole locations are labeled and circled by dashed circles. (f) Experimentally acquired reciprocal space structure of the monolayer graphene on a twinned Cu(111) film.

thermal annealing and graphene growth is very sensitive to the sapphire substrate's surface pretreatment, the Cu sputtering parameters, and the thermal annealing conditions.[24,25] Any small parameter fluctuations will cause the failure of the single crystal Cu formation. In our work, more than 50% Cu films on sapphire remain to be twinned while we try our best to minimize the variation of processing conditions. The situation may become worse if the sapphires are recycled for sputter deposition of Cu. In contrast, for the Cu film sputtered on spinel(111), it is consistently found to be twin-free after the thermal annealing and graphene growth. The SEM and EBSD data for this case can be found in Figure S5.

Figure 3a shows the optical image of a continuous graphene (10 mm × 10 mm) sheet transferred to a $SiO_2$(50 nm)/Si substrate. The edge area of graphene (bottom portion of Figure 3a) is intentionally covered in this image for contrast. Five Raman spectra were randomly collected on this graphene sheet. Figure 3b shows that all spectra indicate the graphene to be monolayer in light of the peak area intensity ratio of 2D/G (4.10 ± 0.36). Different from the pretransferred counterparts, these post-transferred spectra have the so-called defect D peak present in each of them,[48,49] probably resulting from the transfer process. The D, G, and 2D peak positions for this transferred graphene are 1344 ± 3, 1588 ± 2, and 2683 ± 6 cm$^{-1}$, respectively. Another difference between the pre- and post-transferred Raman spectra is the substantial red-shift of the 2D peak, from the pretransferred to post-transferred. This may be related to the strain during graphene growth on Cu(111) surface. The SEM image of the transferred graphene is shown in Figure 3c. It can be seen that the image is dominated by the light gray color which represents the monolayer graphene. Under the view, there are indeed a few dark gray flakes corresponding to multilayer graphene, but the fraction of these features is too small to be significant. Also, the size of these flakes is small (1−2 $\mu$m) and undetectable by the Raman spectroscopy. In addition, line features can be clearly observed in Figure 3c. Two reasons lead us to believe these lines are the wrinkles formed during graphene's relaxation on the $SiO_2$/Si substrates, rather than grain boundaries or boundaries of other kinds. The first reason will be elaborated with the aid of RHEED results in the next section, where it is shown that the transferred graphene is single-crystalline and should be free of large-angle grain boundary. The second reason is from the AFM scanning on these lines. The AFM image in Figure 3d reveals the details of these lines, which seem to be an outcome of graphene buckling. Further evidence comes from Figure 3e. The zoom-in line profiles across these features are quite smooth with small slopes of ~0.13 (~7.45°), indicating the features are more likely to be wrinkles that are intrinsic to graphene.[50,51]

The symmetry and perfection of the pretransferred graphene are usually determined by the LEED technique.[52,53] Alternatively, we have reported that RHEED is capable of revealing the symmetry of the graphene structure as well by constructing the reciprocal space mapping of graphene.[34] For a single-crystalline two-dimensional (2D) material, its reciprocal space structure consists of vertical rods.[54,55] Due to the relatively large wave vector of the electrons in RHEED, the Ewald sphere is large and cuts through the rods in the reciprocal space like a plane. As a result, streaks would form in RHEED patterns for 2D materials. By measuring the characteristics of streaks as a function of the momentum transfer ($\boldsymbol{k} = \boldsymbol{k}_{out} - \boldsymbol{k}_{in}$, where $\boldsymbol{k}_{out}$ and $\boldsymbol{k}_{in}$ are the wave vectors of outgoing and incident electrons) parallel to the surface ($\boldsymbol{k}_{\parallel}$) while varying the azimuthal angle $\varphi$, the reciprocal space structure of a 2D material can be obtained. First, we show in Figures 4a and b a pair of RHEED patterns acquired from a monolayer graphene on a twin-free Cu(111) film at two representative $\varphi$ of 0 and 30.6°, respectively. The central streak represents the (00) lattice of the reciprocal space of graphene, while additional streaks come from the nonzero $\boldsymbol{k}_{\parallel}$ vectors $\vec{G}$ ($hk$) in the reciprocal space. The corresponding


DOI: 10.1021/acsami.7b01370
ACS Appl. Mater. Interfaces XXXX, XXX, XXX−XXX

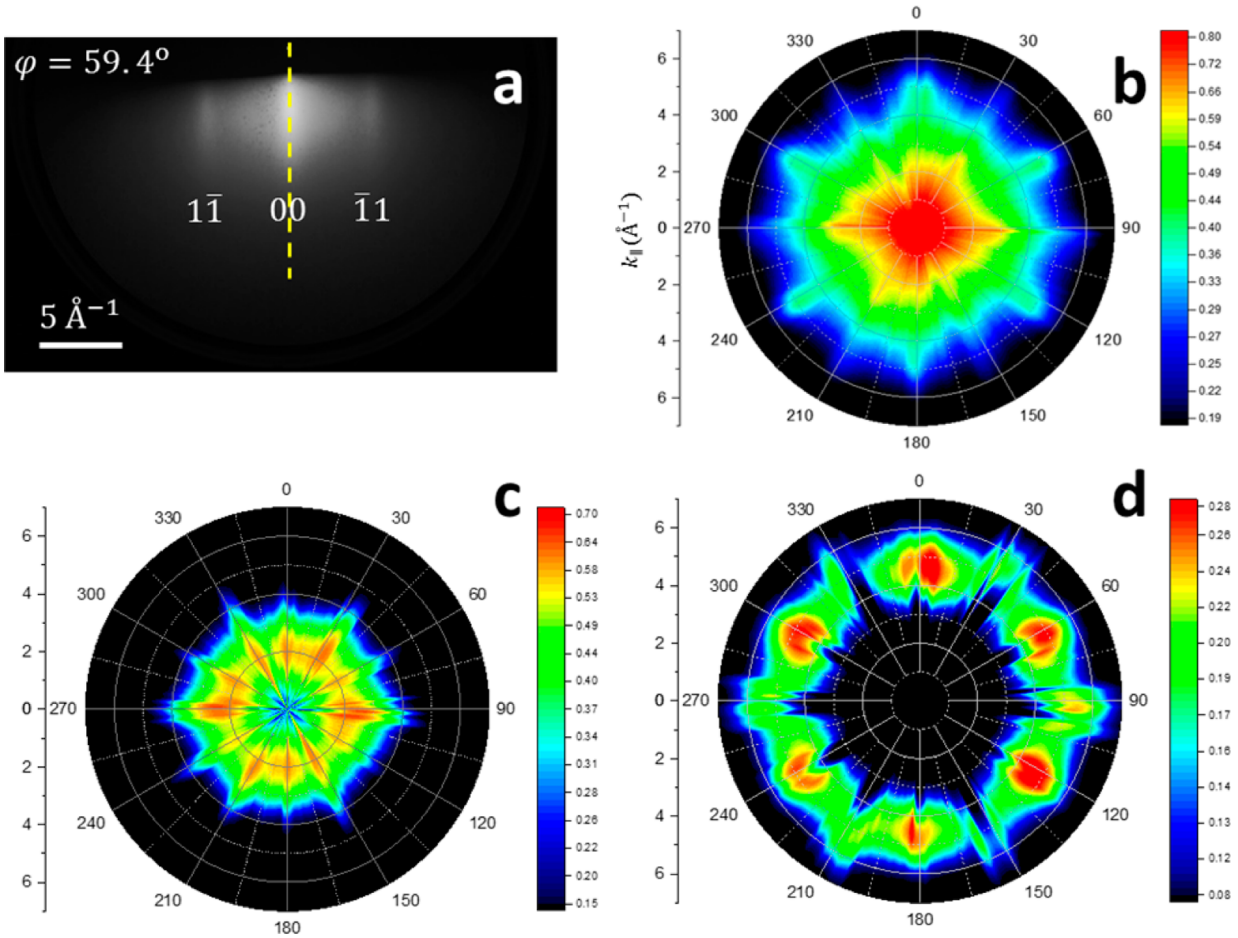


**Figure 5.** (a) RHEED pattern of the monolayer graphene transferred to a $SiO_2$/Si substrate collected at the azimuthal angle $\varphi$ = 59.4°. (b) Experimentally acquired reciprocal space structure of the monolayer graphene transferred to a $SiO_2$/Si substrate. (c, d) Decomposition of (b) to show (c) inner six spots and (d) outer six spots.

indexing of streaks can be found in Figures 4a and b. The directions of the line intensity profile scans, blue in Figure 4a and red in Figure 4b, are illustrated in Figure 4c, where $\vec{b}_1$ and $\vec{b}_2$ are the primitive vectors in the reciprocal space of graphene. Figure 4d shows the intensity profiles of these line scans as a function of $\boldsymbol{k}_{\parallel}$ (the distances from $(hk)$ to (00)) at a fixed perpendicular momentum transfer $\boldsymbol{k}_{\perp}$. With these measurements, we can experimentally determine $|\vec{b}_1| = |\vec{b}_2| = 2.95 \pm 0.05$ Å$^{-1}$, which agrees very well with that of graphene reported in the literature.[56]

Next, to investigate the in-plane crystallography of this graphene, we construct its 2D reciprocal space structure by collecting 100 RHEED patterns from 100 azimuthal angles (from 0 to 180°, step size 1.8°). We first measure the intensity profile at each angle and then plot the azimuthal angle-dependent intensity profile in a polar coordinate system. In this 2D reciprocal space structure, the radius represents the reciprocal distance from the (00) spot and the polar angle represents the azimuthal angle. Figure 4e shows the reciprocal space structure of the monolayer graphene on a twin-free Cu(111) film. In this figure, there are clearly six symmetrical spots, namely, (21), (12), $(\bar{1}1)$, $(2\bar{1})$, $(1\bar{2})$, and $(1\bar{1})$, at a reciprocal distance of 5.1 Å$^{-1}$ from the center. In addition, at a shorter reciprocal distance of 2.9 Å$^{-1}$, there are six more symmetrical spots, namely, (10), (11), (01), $(\bar{1}0)$, $(\bar{1}\bar{1})$, and $(0\bar{1})$, each rotated 30° in the azimuthal angle with respect to the previous set. The symmetry and the position of these spots agree with the theoretical calculation on a single-crystalline graphene. Thus, the graphene under investigation is indeed in single-crystalline form. Furthermore, we construct the reciprocal space structure of the monolayer graphene on a twinned Cu(111) film, shown in Figure 4f. Previous studies[20,53] reported that the graphene growth direction is rotated 30° when crossing the 60° in-plane twin boundaries. In this study, however, no additional rotational spots can be found in Figure 4f besides those can be indexed similarly as in Figure 4e. In other words, the graphene grown on twinned Cu(111) films is in single-crystalline form without additional 30° rotation domains caused by the twin boundaries. It is possible that in our present experiment, the graphene growth direction is rotated 60° in-plane at the Cu twin boundaries in response to their interruption. Since graphene is 6-fold symmetric, this 60° rotation is equivalent to no rotation in terms of in-plane orientation. However, we cannot exclude the possibility of a small fraction of graphene that gets rotated non-60° at the twin boundaries due to the finite resolution of the current technique, but this should not affect our conclusion regarding twin boundary drawn in this work, since about 50% area of the Cu films are twinned, which is well within the detection ability of azimuthal RHEED.

While harmless to in-plane crystal orientation, the twin boundaries do affect the graphene growth in some other ways.


DOI: 10.1021/acsami.7b01370
ACS Appl. Mater. Interfaces XXXX, XXX, XXX−XXX

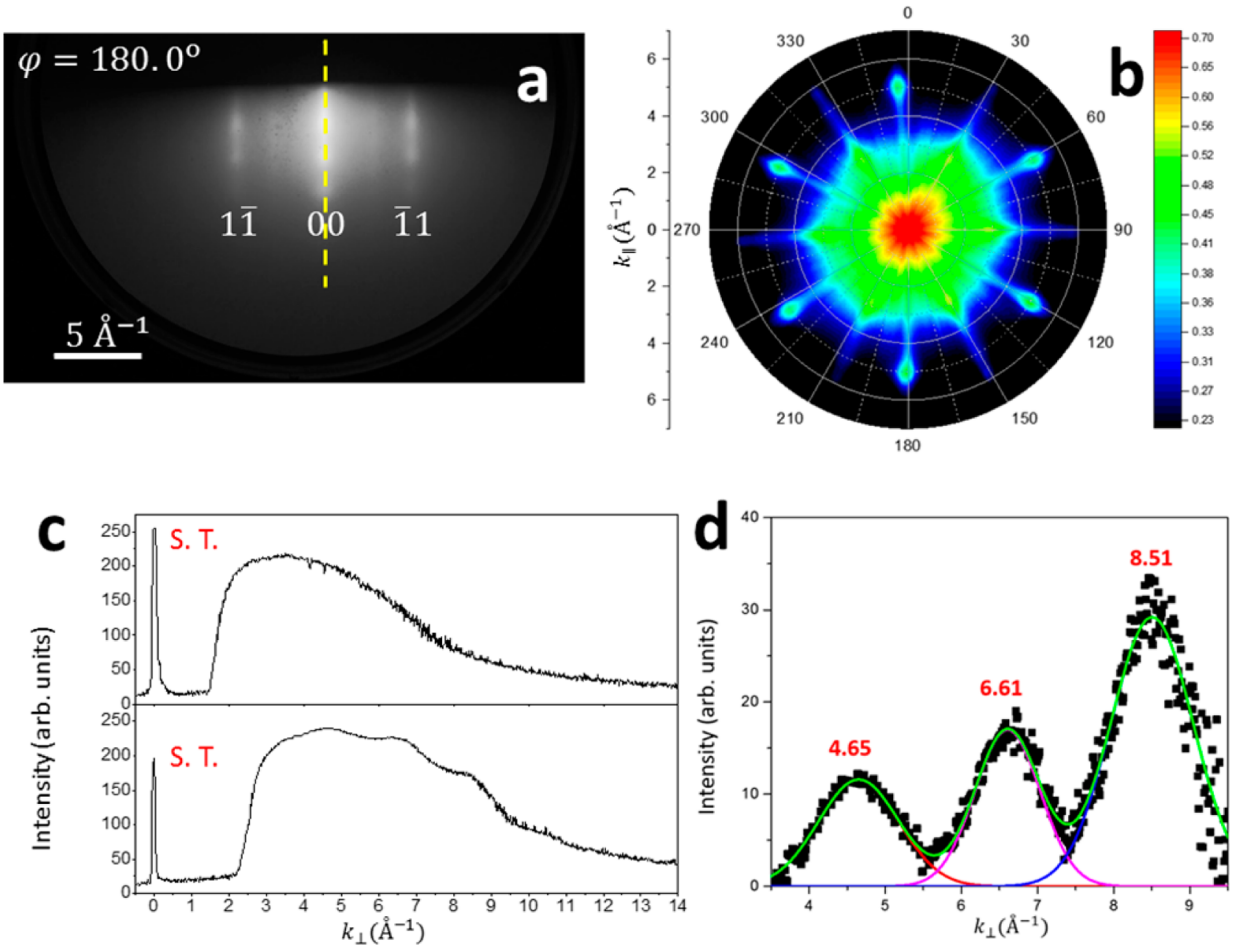


**Figure 6.** (a) RHEED pattern of the multilayer graphene transferred to a $SiO_2$/Si substrate collected at the azimuthal angle $\varphi$ = 180°. (b) Experimentally acquired reciprocal space structure of the multilayer graphene transferred to a $SiO_2$/Si substrate. (c) Intensity profiles vs momentum transfer perpendicular to the substrate ($k_{\perp}$) along the yellow dashed lines in RHEED patterns shown in Figure 5a and (a). S.T. stands for the straight through incident electron beam landed on the phosphorus screen. (d) Peak fitting of the intensity profile in the lower part of (c) after background subtraction.

Parts a and b of Figure S6 show the optical images of post-transferred bilayer and multilayer graphene grown on twinned Cu(111) films. Overall, the bilayer and multilayer graphene flakes are scattered everywhere on the monolayer graphene base, but they appear to have a preference in selecting locations. The blue dashed lines in Figure S6a,b are guides of graphene morphology to the eyes. It is seen that graphene tends to grow into bilayer or multilayer along these dashed lines. After checking the size and shape of these lines, it can be recognized that the lines reflect the twin boundaries in the Cu films. Figure 2e can be used as a reference. Thus, we believe the twin boundaries tend to serve as nucleation sites for graphene to grow into multilayer. This is not unexpected, given the feature of twin boundaries. In Figure 2d, one can see that the twin boundaries are essentially grooves with multiple steps. From the thermodynamics perspective of materials, the features such as steps are particularly favorable for materials to nucleate. It is no exception for graphene when it comes to nucleation on Cu(111).[57]

What makes this azimuthal RHEED technique more appealing is that it can be used to determine the symmetry of graphene even after the graphene is transferred to $SiO_2$/Si substrates, which carries a special significance from the perspective of making graphene-based electronic devices. Parts a and b of Figure 5 show a representative RHEED pattern and the reciprocal space structure of a monolayer graphene transferred to a $SiO_2$/Si substrate, respectively. There appears to be a spread in the streaks in Figure 5a and, in turn, in the spots in Figure 5b. To better view, we decompose the mapping of Figure 5b into two separate regimes representing the inner and outer spots as shown in parts c and d, respectively, of Figure 5. In each mapping, especially the latter, the 6-fold symmetry of single-crystalline graphene can be visualized again, suggesting the crystallographic property of post-transferred graphene can be preserved. The spread of the spots for this sample is probably due to the electron scattering from the wrinkles, similar to that observed on the broadening of the TEM diffraction beams from a graphene layer.[58] We also use azimuthal RHEED to study the structure of a multilayer graphene transferred to a $SiO_2$/Si substrate. The representative RHEED pattern and reciprocal space structure of this sample are shown in parts a and b, respectively, of Figure 6. Compared to Figure 5b, Figure 6b displays much sharper spots. This is due to the decreasing of wrinkle density in multilayer graphene. Unlike single-layer graphene, multilayer graphene can stabilize itself without creating too many wrinkles. The SEM image and Raman spectra of this multilayer graphene can be found in Figure S7. Also note that the multilayer graphene is still in


DOI: 10.1021/acsami.7b01370
ACS Appl. Mater. Interfaces XXXX, XXX, XXX−XXX

single-crystalline form per Figure 6b. In fact, Figure 6b may represent what a single-crystalline graphite would produce. According to ref 59 and the simulation of graphite's $\{10\bar{1}1\}$ pole figure projected onto the (0001) plane (Figure S8), a single-crystalline graphite indeed has a 6-fold symmetry. In summary, we believe the graphite-like multilayer graphene gives rise to the sharp RHEED patterns and thus a sharp reciprocal space structure, but monolayer graphene has difficulty doing so because it contains many wrinkles.

In the representative RHEED patterns of the monolayer graphene (Figure 5a) and the multilayer graphene (Figure 6a), one can see that each streak for the monolayer graphene is continuous along vertical direction, while beading can be observed on the streaks for the multilayer graphene. This is caused by the change in reciprocal space structure from monolayer to multilayer graphene.[54] Here, we plot the intensity profiles along the central streaks as indicated by the yellow dashed lines. Shown in Figure 6c, the intensity profile is smooth for the monolayer graphene, but oscillates for the multilayer graphene. After using the profile of monolayer graphene as the background for subtraction, we resolve the oscillation curve with a period of $\Delta = 1.93 \pm 0.04$ Å$^{-1}$ for the multilayer, shown in Figure 6d. The oscillation implies that this graphene contains multiple layers whose interlayer spacing ($d$) in real space can be estimated to be $d = 2\pi/\Delta = 3.27 \pm 0.07$ Å. Note that the interplanar distance between graphite's layers is 3.35 Å, close to the $d$ value we extract from the multilayer graphene. Therefore, it suggests that the RHEED technique is also able to probe the crystallographic properties of multilayer graphene along the out-of-plane direction.

Last, we make some remarks on our graphene growth and the azimuthal RHEED method. The quality of our graphene is competitive, as evidenced by the single crystallinity and wafer-scale integrity (scalable and only limited by the size of the substrate used). While the synthesis of wafer-scale single crystalline graphene has already been reported, highly expensive substrates, such as single crystalline germanium wafers and single crystalline silicon carbide wafers, usually have to be used in those works.[3,60] Our work presents a cost-effective route via single-crystalline Cu(111) buffered sapphire or spinel wafers to the same destination. What's more, our work suggests that the 60° in-plane twinning of Cu(111) should not cause too much concern on the crystalline integrity of graphene. Thus, Cu(111) films should be suitable to grow single crystalline graphene, if the twinning of Cu is in-plane and at 60°. The shortcoming of our graphene, like most wet-transferred graphene, lies in the wrinkles. Regarding the comparison between LEED and our azimuthal RHEED for graphene studies, there are pros and cons in each. When graphene is on conductive substrates, LEED is certainly more powerful. LEED is simpler in that the electron beam incidents on the area of interest and gets the diffraction pattern of graphene directly. In azimuthal RHEED, a large number of patterns between $\varphi = 0°$ and 360° have to be collected to construct the reciprocal space mapping of graphene and then reveal the crystallinity. Also, LEED can directly tell the epitaxial alignment of graphene on the substrate. In azimuthal RHEED, this is also doable, but has to be done in a more complex manner by keeping track of the geometry of graphene sheet since the graphene is already transferred out of the original substrate. However, for graphene on some insulating substrates, it is a completely different story. The proposed azimuthal RHEED method in this work becomes more powerful in this scenario as LEED is not suitable.

## CONCLUSIONS

In summary, we report the wafer-scale growth of single-crystalline graphene on single-crystalline Cu(111) films with a low pressure CVD method. After the thermal annealing and the graphene growth, it is found that the Cu(111) film sputtered on spinel(111) substrates turns into a single crystal, while the Cu(111) film sputtered on sapphire(0001) gives rise to mixed results, sometimes twin-free single crystals and sometimes twinned crystals. Interestingly, the symmetry study with azimuthal RHEED reveals that the graphene, whether grown on twin-free or twinned Cu(111) films, is in single-crystalline form. This finding leads us to conclude that the 60° in-plane rotational twinning in Cu(111) films does not alter the symmetry of graphene grown atop. However, the twin boundaries do affect the graphene growth by serving as nucleation sites for multilayer graphene growth. Most importantly, in this work, we verify the feasibility of using azimuthal RHEED method to determine the symmetry of post-transferred and large area graphene on $SiO_2$/Si substrates, which represents an important step toward better understanding the structure of graphene before using it to make large area devices.

## EXPERIMENTAL SECTION

About 900 nm thick Cu films were epitaxially grown on sapphire(0001) and spinel(111) substrates, both substrates from MTI Corp., using DC sputtering. Sapphire or spinel substrates (10 mm × 10 mm × 0.5 mm) were first cleaned using a sonication method in methanol for 20 min and then immersed in piranha solution ($H_2O_2$ (35%)/$H_2SO_4$ (96%) = 1:1) and diluted Aqua regia solution (HCl (35%)/$HNO_3$/$H_2O$ = 3:1:2), for 10 min, respectively, to remove the trace organic and metal contaminants. The substrates were further cleaned in RCA SC1 solution ($H_2O$/$H_2O_2$/$NH_4OH$ = 5:1:1) and SC2 solution ($H_2O$/$H_2O_2$/HCl = 5:1:1), for 10 min at 55 °C, respectively, then rinsed in deionized water for 10 min and dried using nitrogen gas.

After cleaning, the substrates were immediately loaded in the sputtering chamber (AJA Orion sputtering system) which had been seasoned with ∼4 μm Cu coating to prevent cross contamination. The base vacuum of this system was $1.0 \times 10^{-7}$ Torr or less. The substrates were preheated to 250 °C and maintained for 15 min for the temperature to stabilize. The sputtering was conducted with the target power of 100 W, working pressure of 3.0 mTorr, and 15 sccm Ar gas flow. A commercial 2-in. polycrystalline Cu sputtering target with a purity of 99.99% was used in this work. The sputtering rate was maintained at ∼3.3 Å/s. After the deposition, the substrates were naturally cooled to room temperature.

The thermal annealing of the as-deposited Cu films and the graphene growth were conducted in the same low pressure CVD furnace (MTI Corporation OTF-1200x). The furnace was designed with a 6 in. × 56 in. quartz tube and three temperature zones. The Cu film substrates were placed in a ceramic boat and covered with a sheet of 25 μm polycrystalline Cu foil (99.98% in purity, Sigma-Aldrich) with small openings, in order to reduce the Cu sublimation at high temperature and control the gas diffusion rate on the sample surface.[61,62] The CVD system was pumped down to ∼50 mTorr and purged with high purity Ar gas. This flushing procedure was repeated three times. Then the system pressure was slowly increased to 50 ± 5 Torr by adjusting the pressure valve during temperature ramping up. In the meantime, 200 sccm Ar and 35 sccm $H_2$ were kept feeding through the tube. After ∼40 min, the temperature ramped up to the anneal temperature of 1020 °C. The annealing time was 15 min.

After thermal annealing, the graphene growth was activated at 1020 °C by introducing methane ($CH_4$, 10 sccm) into the furnace. In a typical run, the graphene growth time was 30 min. After the growth, the $CH_4$ gas feed was immediately turned off. The furnace lid was opened to allow rapid cooling. Meanwhile the Ar and $H_2$ gases were kept flowing until the furnace cooled to room temperature.


DOI: 10.1021/acsami.7b01370
ACS Appl. Mater. Interfaces XXXX, XXX, XXX−XXX

The graphene transfer followed the standard poly(methyl methacrylate) (PMMA, MicroChem 950 A4)-mediated method.[27,28] In brief, the graphene surface was spin-coated five times with PMMA (spun at 1500 rpm for 60 s and baked at 120 °C for 10 min in between each spin coating) and then immersed in the ammonium persulfate solution (3.0 g in 50 mL of deionized water) for 24−48 h to dissolve the Cu. Note the Cu film was sandwiched in between sapphire/spinel and PMMA. As a result, the etching was diffusion-limited and took longer than those using Cu foils as substrates. Once released from Cu, the PMMA−graphene stack was rinsed several times in deionized water and then scooped out using a precleaned silicon wafer with 50 nm thermal oxide. The PMMA−graphene−substrate stack was dried in air and baked at 150 °C for 15 min, followed by dissolving the PMMA protection film in acetone. Finally, the graphene film was rinsed with 2-propanol and dried with nitrogen gas. It should be noted that after Cu is completely etched, the sapphire and spinel substrates can be reused as long as they are thoroughly cleaned as described earlier.

SEM (Karl Zeiss Ultra 1540 EsB system) and AFM (Park Scientific Autoprobe CP, Dimension 3100, Veeco Instruments) were used to characterize the surface morphology. XRD (Bruker D8-Discover system) and EBSD (NordlysNano Detector, Oxford Instruments integrated with the Karl Zeiss Ultra 1540 EsB system) were used to characterize the crystallographic properties of the Cu film. The XRD $\theta$-$2\theta$, rocking curve and pole figure scans were conducted using a Cu K$\alpha$ radiation source ($\lambda$ = 1.54 Å). For EBSD characterization, a 15 kV electron beam was used to scan surface areas with a size of 1500 × 1100 $\mu$m, 110 × 100 $\mu$m, 20 × 20 $\mu$m and 5.0 × 5.0 $\mu$m using a working distance of 18 mm. The scan step size was set at 20 $\mu$m, 5 $\mu$m, 500 nm, and 100 nm, respectively. The crystallographic orientation data was collected using the Aztec EBSD data acquisition software and postanalyzed using the HKL Channel 5 package (Oxford Instruments) for crystallographic orientation mapping and pole figure/inverse pole figure (IPF) plotting. Raman spectroscopy (Renishaw model 2000A, $\lambda$ = 514 nm) was used to characterize the graphene, both pre- and post-transfer. The laser spot was ∼5.0 $\mu$m in size. Typically, the measurements were conducted with 10 s integration time and 5 accumulations. Peak fitting was performed using Lorentz function. For RHEED, the graphene samples were loaded into the RHEED chamber without any prior treatment. The RHEED system consists of an electron gun (model RDA-003G) which generates a 20 keV electron beam incident at a glancing angle of ∼1° on the sample surface. The emission current used was 45 $\mu$A. The RHEED pattern was projected on a phosphor screen mounted on a 6 in. flange which was about 20 cm away from the sample in a vacuum chamber with a base pressure of $10^{-8}$ Torr. The RHEED pattern was captured by a digital camera positioned outside the chamber facing the phosphor screen. The sample was mounted on a holder with the sample's azimuthal rotation controlled by a stepper motor. In order to probe the entire upper half of the reciprocal space, the sample was rotated azimuthally with a 1.8° step size from 0° to 180° in 100 steps and the corresponding RHEED pattern was recorded at each incremental step. It is noted that the azimuthal angle $\varphi$ is relative. For a single crystalline graphene, RHEED patterns of the same family should be visible at only six $\varphi$ angles in between 0 and 360°, each 60° apart. There are two families of RHEED patterns for a single crystalline graphene. One corresponds to the outer six spots at a reciprocal distance of 5.1 $Å^{-1}$ from the center and the other inner six at 2.9 $Å^{-1}$. Normally, when rotating the sample, we define $\varphi$ to be zero when we first observe a RHEED pattern whether it is from the outer set or inner set. For example, in Figure 4a, we saw a diffraction pattern corresponding to an inner spot, and we defined this as $\varphi$ = 0 for this sample. This diffraction pattern actually reflected the (10) and $(\bar{1}0)$ spots in Figure 4e. Then after a rotation of 30.6°, we saw the second pattern as shown in Figure 4b, corresponding to (21) and $(\bar{2}1)$ spots in Figure 4e. (Note that the step size of rotation was 1.8°, so we cannot have the $\varphi$ angle exactly at integer 30°, although theoretically the pattern should be most visible at 30°. But in an experiment, this did not make too much difference.) In short, the azimuthal angle is relative. This applies to all RHEED data in the present work.

## ■ ASSOCIATED CONTENT

### Supporting Information

The Supporting Information is available free of charge on the ACS Publications website at DOI: 10.1021/acsami.7b01370.

Additional XRD, EBSD, SEM, Raman, and optical characterization results (PDF)

## ■ AUTHOR INFORMATION


### Corresponding Author

*E-mail: sunx12@rpi.edu.

### ORCID

Xin Sun: 0000-0001-5633-3371


### Notes

The authors declare no competing financial interest.

## ■ ACKNOWLEDGMENTS

This work is supported by the NYSTAR Focus Center at RPI, C130117, and by NSF Award under DMR 1305293. We thank Prof. Nikhil Koratkar for allowing us to use the CVD furnace and Prof. Philip I. Cohen for wonderful discussions. We also thank the Micro and Nano Fabrication Clean Room (MNCR) staff at RPI for facilitating the experimental work.

## ■ REFERENCES


(1) Novoselov, K. S.; Geim, A. K.; Morozov, S. V.; Jiang, D.; Zhang, Y.; Dubonos, S. V.; Grigorieva, I. V.; Firsov, A. A. Electric Field Effect in Atomically Thin Carbon Films. *Science* **2004**, *306* (5696), 666−669.

(2) Ago, H.; Ohta, Y.; Hibino, H.; Yoshimura, D.; Takizawa, R.; Uchida, Y.; Tsuji, M.; Okajima, T.; Mitani, H.; Mizuno, S. Growth Dynamics of Single-Layer Graphene on Epitaxial Cu Surfaces. *Chem. Mater.* **2015**, *27* (15), 5377−5385.

(3) Lee, J.-H.; Lee, E. K.; Joo, W.-J.; Jang, Y.; Kim, B.-S.; Lim, J. Y.; Choi, S.-H.; Ahn, S. J.; Ahn, J. R.; Park, M.-H.; Yang, C.-W.; Choi, B. L.; Hwang, S.-W.; Whang, D. Wafer-Scale Growth of Single-Crystal Monolayer Graphene on Reusable Hydrogen-Terminated Germanium. *Science* **2014**, *344* (6181), 286−289.

(4) Mun, J. H.; Cho, B. J. Synthesis of Monolayer Graphene Having a Negligible Amount of Wrinkles by Stress Relaxation. *Nano Lett.* **2013**, *13* (6), 2496−2499.

(5) Pan, Y.; Zhang, H.; Shi, D.; Sun, J.; Du, S.; Liu, F.; Gao, H.-j. Highly Ordered, Millimeter-Scale, Continuous, Single-Crystalline Graphene Monolayer Formed on Ru (0001). *Adv. Mater.* **2009**, *21* (27), 2777−2780.

(6) Zhou, H.; Yu, W. J.; Liu, L.; Cheng, R.; Chen, Y.; Huang, X.; Liu, Y.; Wang, Y.; Huang, Y.; Duan, X. Chemical Vapour Deposition Growth of Large Single Crystals of Monolayer and Bilayer Graphene. *Nat. Commun.* **2013**, *4*, 2096.

(7) Yan, Z.; Lin, J.; Peng, Z.; Sun, Z.; Zhu, Y.; Li, L.; Xiang, C.; Samuel, E. L.; Kittrell, C.; Tour, J. M. Toward the Synthesis of Wafer-Scale Single-Crystal Graphene on Copper Foils. *ACS Nano* **2012**, *6* (10), 9110−9117.

(8) Mohsin, A.; Liu, L.; Liu, P.; Deng, W.; Ivanov, I. N.; Li, G.; Dyck, O. E.; Duscher, G.; Dunlap, J. R.; Xiao, K.; Gu, G. Synthesis of Millimeter-Size Hexagon-Shaped Graphene Single Crystals on Resolidified Copper. *ACS Nano* **2013**, *7* (10), 8924−8931.

(9) Lee, Y.; Bae, S.; Jang, H.; Jang, S.; Zhu, S.-E.; Sim, S. H.; Song, Y. I.; Hong, B. H.; Ahn, J.-H. Wafer-Scale Synthesis and Transfer of Graphene Films. *Nano Lett.* **2010**, *10* (2), 490−493.

(10) Nguyen, V. L.; Perello, D. J.; Lee, S.; Nai, C. T.; Shin, B. G.; Kim, J.-G.; Park, H. Y.; Jeong, H. Y.; Zhao, J.; Vu, Q. A.; Lee, S. H.; Loh, K. P.; Jeong, S.-Y.; Lee, Y. H. Wafer-Scale Single-Crystalline AB-Stacked Bilayer Graphene. *Adv. Mater.* **2016**, *28* (37), 8177−8183.

(11) Lee, S.; Lee, K.; Zhong, Z. Wafer Scale Homogeneous Bilayer Graphene Films by Chemical Vapor Deposition. *Nano Lett.* **2010**, *10* (11), 4702−4707.




DOI: 10.1021/acsami.7b01370
ACS Appl. Mater. Interfaces XXXX, XXX, XXX−XXX

(12) Ta, H. Q.; Perello, D. J.; Duong, D. L.; Han, G. H.; Gorantla, S.; Nguyen, V. L.; Bachmatiuk, A.; Rotkin, S. V.; Lee, Y. H.; Rümmeli, M. H. Stranski−Krastanov and Volmer−Weber CVD Growth Regimes To Control the Stacking Order in Bilayer Graphene. *Nano Lett.* **2016**, *16* (10), 6403−6410.
(13) Zhang, Y.; Tang, T.-T.; Girit, C.; Hao, Z.; Martin, M. C.; Zettl, A.; Crommie, M. F.; Shen, Y. R.; Wang, F. Direct Observation of a Widely Tunable Bandgap in Bilayer Graphene. *Nature* **2009**, *459* (7248), 820−823.
(14) Wang, H.; Xu, X.; Li, J.; Lin, L.; Sun, L.; Sun, X.; Zhao, S.; Tan, C.; Chen, C.; Dang, W.; Ren, H.; Zhang, J.; Deng, B.; Koh, A. L.; Liao, L.; Kang, N.; Chen, Y.; Xu, H.; Ding, F.; Liu, K.; Peng, H.; Liu, Z. Surface Monocrystallization of Copper Foil for Fast Growth of Large Single-Crystal Graphene under Free Molecular Flow. *Adv. Mater.* **2016**, *28* (40), 8968−8974.
(15) Addou, R.; Dahal, A.; Sutter, P.; Batzill, M. Monolayer Graphene Growth on Ni(111) by Low Temperature Chemical Vapor Deposition. *Appl. Phys. Lett.* **2012**, *100* (2), 021601.
(16) Ago, H.; Ito, Y.; Mizuta, N.; Yoshida, K.; Hu, B.; Orofeo, C. M.; Tsuji, M.; Ikeda, K.-I.; Mizuno, S. Epitaxial Chemical Vapor Deposition Growth of Single-Layer Graphene over Cobalt Film Crystallized on Sapphire. *ACS Nano* **2010**, *4* (12), 7407−7414.
(17) Coraux, J.; N'Diaye, A. T.; Busse, C.; Michely, T. Structural Coherency of Graphene on Ir(111). *Nano Lett.* **2008**, *8* (2), 565−570.
(18) Zhao, L.; Rim, K. T.; Zhou, H.; He, R.; Heinz, T. F.; Pinczuk, A.; Flynn, G. W.; Pasupathy, A. N. Influence of Copper Crystal Surface on the CVD Growth of Large Area Monolayer Graphene. *Solid State Commun.* **2011**, *151* (7), 509−513.
(19) Ogawa, Y.; Hu, B.; Orofeo, C. M.; Tsuji, M.; Ikeda, K.-I.; Mizuno, S.; Hibino, H.; Ago, H. Domain Structure and Boundary in Single-Layer Graphene Grown on Cu(111) and Cu(100) Films. *J. Phys. Chem. Lett.* **2012**, *3* (2), 219−226.
(20) Jacobberger, R. M.; Arnold, M. S. Graphene Growth Dynamics on Epitaxial Copper Thin Films. *Chem. Mater.* **2013**, *25* (6), 871−877.
(21) Mattevi, C.; Kim, H.; Chhowalla, M. A Review of Chemical Vapour Deposition of Graphene on Copper. *J. Mater. Chem.* **2011**, *21* (10), 3324−3334.
(22) Katz, G. The Epitaxy of Copper on Sapphire. *Appl. Phys. Lett.* **1968**, *12* (5), 161−163.
(23) Takesaki, Y.; Kawahara, K.; Hibino, H.; Okada, S.; Tsuji, M.; Ago, H. Highly Uniform Bilayer Graphene on Epitaxial Cu−Ni(111) Alloy. *Chem. Mater.* **2016**, *28* (13), 4583−4592.
(24) Verguts, K.; Vermeulen, B.; Vrancken, N.; Schouteden, K.; Van Haesendonck, C.; Huyghebaert, C.; Heyns, M.; De Gendt, S.; Brems, S. Epitaxial $Al_2O_3$(0001)/Cu(111) Template Development for CVD Graphene Growth. *J. Phys. Chem. C* **2016**, *120* (1), 297−304.
(25) Miller, D. L.; Keller, M. W.; Shaw, J. M.; Rice, K. P.; Keller, R. R.; Diederichsen, K. M. Giant Secondary Grain Growth in Cu Films on Sapphire. *AIP Adv.* **2013**, *3* (8), 082105.
(26) Gamo, Y.; Nagashima, A.; Wakabayashi, M.; Terai, M.; Oshima, C. Atomic Structure of Monolayer Graphite Formed on Ni(111). *Surf. Sci.* **1997**, *374* (1), 61−64.
(27) Liang, X.; Sperling, B. A.; Calizo, I.; Cheng, G.; Hacker, C. A.; Zhang, Q.; Obeng, Y.; Yan, K.; Peng, H.; Li, Q.; Zhu, X.; Yuan, H.; Hight Walker, A. R.; Liu, Z.; Peng, L.-M.; Richter, C. A. Toward Clean and Crackless Transfer of Graphene. *ACS Nano* **2011**, *5* (11), 9144−9153.
(28) Li, X.; Zhu, Y.; Cai, W.; Borysiak, M.; Han, B.; Chen, D.; Piner, R. D.; Colombo, L.; Ruoff, R. S. Transfer of Large-Area Graphene Films for High-Performance Transparent Conductive Electrodes. *Nano Lett.* **2009**, *9* (12), 4359−4363.
(29) Wei, D.; Lu, Y.; Han, C.; Niu, T.; Chen, W.; Wee, A. T. S. Critical Crystal Growth of Graphene on Dielectric Substrates at Low Temperature for Electronic Devices. *Angew. Chem., Int. Ed.* **2013**, *52* (52), 14121−14126.
(30) Chen, X.-D.; Chen, Z.; Jiang, W.-S.; Zhang, C.; Sun, J.; Wang, H.; Xin, W.; Lin, L.; Priydarshi, M. K.; Yang, H.; Liu, Z.-B.; Tian, J.-G.; Zhang, Y.; Zhang, Y.; Liu, Z. Fast Growth and Broad Applications of 25-Inch Uniform Graphene Glass. *Adv. Mater.* **2017**, *29* (1), 1603428.
(31) Chen, J.; Guo, Y.; Wen, Y.; Huang, L.; Xue, Y.; Geng, D.; Wu, B.; Luo, B.; Yu, G.; Liu, Y. Two-Stage Metal-Catalyst-Free Growth of High-Quality Polycrystalline Graphene Films on Silicon Nitride Substrates. *Adv. Mater.* **2013**, *25* (7), 992−997.
(32) Pang, J.; Mendes, R. G.; Wrobel, P. S.; Wlodarski, M. D.; Ta, H. Q.; Zhao, L.; Giebeler, L.; Trzebicka, B.; Gemming, T.; Fu, L.; Liu, Z.; Eckert, J.; Bachmatiuk, A.; Rümmeli, M. H. Self-Terminating Confinement Approach for Large-Area Uniform Monolayer Graphene Directly over Si/SiOx by Chemical Vapor Deposition. *ACS Nano* **2017**, *11*, 1946.
(33) Huang, P. Y.; Ruiz-Vargas, C. S.; van der Zande, A. M.; Whitney, W. S.; Levendorf, M. P.; Kevek, J. W.; Garg, S.; Alden, J. S.; Hustedt, C. J.; Zhu, Y.; Park, J.; McEuen, P. L.; Muller, D. A. Grains and Grain Boundaries in Single-Layer Graphene Atomic Patchwork Quilts. *Nature* **2011**, *469* (7330), 389−392.
(34) Xiang, Y.; Guo, F.-W.; Lu, T.-M.; Wang, G.-C. Reflection High-Energy Electron Diffraction Measurements of Reciprocal Space Structure of 2D Materials. *Nanotechnology* **2016**, *27* (48), 485703.
(35) Satapathy, D. K.; Jenichen, B.; Ploog, K. H.; Braun, W. Azimuthal Reflection High-Energy Electron Diffraction Study of MnAs Growth on GaAs(001) by Molecular Beam Epitaxy. *J. Appl. Phys.* **2011**, *110* (2), 023505.
(36) Touzin, M.; Goeuriot, D.; Guerret-Piécourt, C.; Juvé, D.; Tréheux, D.; Fitting, H.-J. Electron Beam Charging of Insulators: A Self-Consistent Flight-Drift Model. *J. Appl. Phys.* **2006**, *99* (11), 114110.
(37) Cazaux, J. Secondary Electron Emission and Charging Mechanisms in Auger Electron Spectroscopy and Related E-Beam Techniques. *J. Electron Spectrosc. Relat. Phenom.* **2010**, *176* (1−3), 58−79.
(38) Estrup, P. J.; McRae, E. G. Surface Studies by Electron Diffraction. *Surf. Sci.* **1971**, *25* (1), 1−52.
(39) Li, X.; Cai, W.; An, J.; Kim, S.; Nah, J.; Yang, D.; Piner, R.; Velamakanni, A.; Jung, I.; Tutuc, E.; Banerjee, S. K.; Colombo, L.; Ruoff, R. S. Large-Area Synthesis of High-Quality and Uniform Graphene Films on Copper Foils. *Science* **2009**, *324* (5932), 1312−1314.
(40) Schwierz, F. Graphene Transistors. *Nat. Nanotechnol.* **2010**, *5* (7), 487−496.
(41) Chen, Z.; Lin, Y.-M.; Rooks, M. J.; Avouris, P. Graphene Nano-Ribbon Electronics. *Phys. E* **2007**, *40* (2), 228−232.
(42) Chen, F.; Xia, J.; Ferry, D. K.; Tao, N. Dielectric Screening Enhanced Performance in Graphene FET. *Nano Lett.* **2009**, *9* (7), 2571−2574.
(43) Yang, H.; Heo, J.; Park, S.; Song, H. J.; Seo, D. H.; Byun, K.-E.; Kim, P.; Yoo, I.; Chung, H.-J.; Kim, K. Graphene Barristor, a Triode Device with a Gate-Controlled Schottky Barrier. *Science* **2012**, *336* (6085), 1140−1143.
(44) Lin, Y.-M.; Valdes-Garcia, A.; Han, S.-J.; Farmer, D. B.; Meric, I.; Sun, Y.; Wu, Y.; Dimitrakopoulos, C.; Grill, A.; Avouris, P.; Jenkins, K. A. Wafer-Scale Graphene Integrated Circuit. *Science* **2011**, *332* (6035), 1294−1297.
(45) Miller, D. L.; Keller, M. W.; Shaw, J. M.; Chiaramonti, A. N.; Keller, R. R. Epitaxial (111) films of Cu, Ni, and CuxNiy on $\alpha$−Al2O3 (0001) for graphene growth by chemical vapor deposition. *J. Appl. Phys.* **2012**, *112* (6), 064317.
(46) Costa, S. D.; Righi, A.; Fantini, C.; Hao, Y.; Magnuson, C.; Colombo, L.; Ruoff, R. S.; Pimenta, M. A. Resonant Raman Spectroscopy of Graphene Grown on Copper Substrates. *Solid State Commun.* **2012**, *152* (15), 1317−1320.
(47) Mooradian, A. Photoluminescence of Metals. *Phys. Rev. Lett.* **1969**, *22* (5), 185−187.
(48) Tuinstra, F.; Koenig, J. L. Raman Spectrum of Graphite. *J. Chem. Phys.* **1970**, *53* (3), 1126−1130.
(49) Ferrari, A. C. Raman Spectroscopy of Graphene and Graphite: Disorder, Electron−Phonon Coupling, Doping and Nonadiabatic Effects. *Solid State Commun.* **2007**, *143* (1−2), 47−57.


DOI: 10.1021/acsami.7b01370
*ACS Appl. Mater. Interfaces* XXXX, XXX, XXX−XXX

(50) Deng, S.; Berry, V. Wrinkled, Rippled and Crumpled Graphene: an Overview of Formation Mechanism, Electronic Properties, and Applications. *Mater. Today* **2016**, *19* (4), 197−212.
(51) Fasolino, A.; Los, J. H.; Katsnelson, M. I. Intrinsic Ripples in Graphene. *Nat. Mater.* **2007**, *6* (11), 858−861.
(52) Robinson, Z. R.; Tyagi, P.; Mowll, T. R.; Ventrice, C. A.; Hannon, J. B. Argon-Assisted Growth of Epitaxial Graphene on Cu(111). *Phys. Rev. B: Condens. Matter Mater. Phys.* **2012**, *86* (23), 235413.
(53) Hu, B.; Ago, H.; Ito, Y.; Kawahara, K.; Tsuji, M.; Magome, E.; Sumitani, K.; Mizuta, N.; Ikeda, K.-I.; Mizuno, S. Epitaxial Growth of Large-Area Single-Layer Graphene over Cu(1 1 1)/Sapphire by Atmospheric Pressure CVD. *Carbon* **2012**, *50* (1), 57−65.
(54) Ichimiya, A.; Cohen, P. *Reflection High-Energy Electron Diffraction*; Cambridge University Press: Cambridge, 2004.
(55) Meyer, J. C.; Geim, A. K.; Katsnelson, M. I.; Novoselov, K. S.; Obergfell, D.; Roth, S.; Girit, C.; Zettl, A. On the Roughness of Single- and Bi-Layer Graphene Membranes. *Solid State Commun.* **2007**, *143* (1−2), 101−109.
(56) Pozzo, M.; Alfè, D.; Lacovig, P.; Hofmann, P.; Lizzit, S.; Baraldi, A. Thermal Expansion of Supported and Freestanding Graphene: Lattice Constant versus Interatomic Distance. *Phys. Rev. Lett.* **2011**, *106* (13), 135501.
(57) Nie, S.; Wofford, J. M.; Bartelt, N. C.; Dubon, O. D.; McCarty, K. F. Origin of the Mosaicity in Graphene Grown on Cu(111). *Phys. Rev. B: Condens. Matter Mater. Phys.* **2011**, *84* (15), 155425.
(58) Meyer, J. C.; Geim, A. K.; Katsnelson, M. I.; Novoselov, K. S.; Booth, T. J.; Roth, S. The Structure of Suspended Graphene Sheets. *Nature* **2007**, *446* (7131), 60−63.
(59) Ferralis, N.; Pussi, K.; Finberg, S. E.; Smerdon, J.; Lindroos, M.; McGrath, R.; Diehl, R. D. Low-Energy Electron Diffraction Study of Potassium Adsorbed on Single-Crystal Graphite and Highly Oriented Pyrolytic Graphite. *Phys. Rev. B: Condens. Matter Mater. Phys.* **2004**, *70* (24), 245407.
(60) Emtsev, K. V.; Bostwick, A.; Horn, K.; Jobst, J.; Kellogg, G. L.; Ley, L.; McChesney, J. L.; Ohta, T.; Reshanov, S. A.; Rohrl, J.; Rotenberg, E.; Schmid, A. K.; Waldmann, D.; Weber, H. B.; Seyller, T. Towards Wafer-Size Graphene Layers by Atmospheric Pressure Graphitization of Silicon Carbide. *Nat. Mater.* **2009**, *8* (3), 203−207.
(61) Li, X.; Magnuson, C. W.; Venugopal, A.; Tromp, R. M.; Hannon, J. B.; Vogel, E. M.; Colombo, L.; Ruoff, R. S. Large-Area Graphene Single Crystals Grown by Low-Pressure Chemical Vapor Deposition of Methane on Copper. *J. Am. Chem. Soc.* **2011**, *133* (9), 2816−2819.
(62) Miseikis, V.; Convertino, D.; Mishra, N.; Gemmi, M.; Mashoff, T.; Heun, S.; Haghighian, N.; Bisio, F.; Canepa, M.; Piazza, V.; Coletti, C. Rapid CVD Growth of Millimetre-Sized Single Crystal Graphene Using a Cold-Wall Reactor. *2D Mater.* **2015**, *2* (1), 014006.


DOI: 10.1021/acsami.7b01370
*ACS Appl. Mater. Interfaces* XXXX, XXX, XXX−XXX